ISSN (Print) 1226-1750
ISSN (Online) 2233-6656
Journal of Magnetics 27(3), 309-314 (2022) https://doi.org/10.4283/JMAG.2022.27.3.309

Distinct Magnetic Properties of $CoFe_2O_4$ by Tetrahedral Mg^{2+} Substitution

Kwang Joo Kim[1], Jongho Park[1], and Jae Yun Park[2]*

[1]*Department of Physics, Konkuk University, Seoul 05029, Republic of Korea*
[2]*Department of Materials Science and Engineering, Incheon National University, Incheon 22012, Republic of Korea*

(Received 20 May 2022, Received in final form 2 September 2022, Accepted 14 September 2022)

Magnetic hysteresis curves of cobalt ferrites with a fraction of cobalt being replaced by magnesium ($Mg_xCo_{1-x}Fe_2O_4$) were investigated by vibrating sample magnetometry (VSM). The specimens with $x \leq 0.2$ were prepared as thin films on silicon substrates by using a sol-gel deposition process. The VSM result revealed that the saturation magnetizations (M_S) of the Mg-substituted specimens were higher than that of $CoFe_2O_4$. The result of Raman spectral analysis suggested that the Mg-substituted specimens had higher tetrahedral Co^{2+} density in the spinel lattice compared to $CoFe_2O_4$. The increase in M_S for $Mg_xCo_{1-x}Fe_2O_4$ is ascribed to two reasons, the increase in tetrahedral Co^{2+} density and significant Mg^{2+} occupation in the tetrahedral sites.

Keywords : cobalt ferrite, magnesium, thin film, magnetic hysteresis, Raman spectroscopy

1. Introduction

Ferrimagnetic transition-metal-oxide compounds have been under a great deal of attention due to their applications as well as physical understanding. As one of the oxides, $CoFe_2O_4$ and its alloys made by substituting Co or Fe ions by other metallic cations are known to have potential applications such as magnetic resonance imaging [1], magneto-mechanical sensing [2], microwave absorption [3], and energy storage [4].

$CoFe_2O_4$ has crystal structure of spinel in which Co^{2+} and Fe^{3+} cations occupy either the 8a (tetrahedral) or the 16d (octahedral) sites surrounded by four and six O^{2-} anions at the 32e sites, respectively. Experimental studies on ferrimagnetic $CoFe_2O_4$ have suggested that the majority of Co^{2+} ions tend to occupy the octahedral (B) sites rather than the tetrahedral (A) sites [5-7] with the intrinsic magnetization being the difference between the antiparallel magnetic moments of the two sites. However, there have been reports in which the Co^{2+} ions exhibited significant A-site occupancy in spinel ferrites [8-11].

The Co^{2+} occupancy in $CoFe_2O_4$ used to be expressed in terms of the inversion parameter δ [8] defined as $(Co^{2+}_{1-\delta}\ Fe^{3+}_{\delta})^A[Co^{2+}_{\delta}\ Fe^{3+}_{2-\delta}]^BO_4$. In case $\delta = 1$, called perfect inverse-spinel, all Co^{2+} ions occupy the B sites, while Fe^{3+} ions occupy A and B sites equally. In theoretical ferrimagnetic state of $CoFe_2O_4$, Co^{2+} and Fe^{3+} ions tend to have magnetic moments of ~3.0 and ~5.0 μ_B, respectively. Thus, for perfect inverse-spinel ($\delta = 1$), net magnetic moment for one formula unit of $CoFe_2O_4$ is estimated to be ~3.0 μ_B. On the other hand, the net magnetic moment for $\delta = 0.7$, where 30 % of Co^{2+} ions occupy A sites, is estimated to be ~4.2 μ_B, being larger than that of $\delta = 1$. So, ferrimagnetic $CoFe_2O_4$ is expected to exhibit an increase in magnetization as the Co^{2+}(A) population increases. Such tetrahedral preference of Co^{2+} ions is likely to vary when other metallic elements occupy the A or B sites for replacing Co^{2+} or Fe^{3+} ions.

The purpose of this work is to investigate the effects of magnesium (Mg) substitution of Co on the structural and magnetic properties of the cobalt ferrites ($CoFe_2O_4 \rightarrow Mg_xCo_{1-x}Fe_2O_4$). The Mg^{2+} substitution in the spinel lattice is likely to affect the distribution of Co^{2+} and Fe^{3+} ions among the A and B sites, altering the physical properties of the cobalt ferrites.

$Mg_xCo_{1-x}Fe_2O_4$ specimens were prepared as thin films by a sol-gel process that is known to be advantageous in controlling chemical composition. The structural properties of the specimens were investigated by X-ray diffraction (XRD), X-ray photoelectron spectroscopy (XPS), and Raman spectroscopy. The magnetic hysteresis curves of the specimens were investigated by vibrating sample magnetometry (VSM). The magnetic evolution of $Mg_xCo_{1-x}Fe_2O_4$ is discussed in comparison with that of

*Corresponding author: Tel: +82-32-835-8271
Fax: +82-32-835-0788, e-mail: pjy@inu.ac.kr

Ca-substituted $Ca_xCo_{1-x}Fe_2O_4$ obtained in a previous study [12]. Although the Mg^{2+} ions are expected to exhibit no magnetic moment, their preference among the 8a and 16d sites in the spinel lattice is likely to affect the magnetic properties of ferrimagnetic $Mg_xCo_{1-x}Fe_2O_4$.

2. Experimental

A series of $Mg_xCo_{1-x}Fe_2O_4$ specimens with $x \leq 0.2$ were prepared through a sol-gel deposition process as follows: (1) Preparation of the precursor solution by dissolving $Fe(NO_3)_3 \cdot 9H_2O$ and $Co(CH_3COO)_2 \cdot 4H_2O$ together in 2-methoxyethanol and ethanolamine at 170 °C for 1 h. For Mg doping $Mg(CH_3COO)_2 \cdot 4H_2O$ was added. (2) Repetition of spin-coating Si(100) substrate using the precursor solution at 3000 rpm for 20 s followed by pre-heating at 300 °C for 5 min. (3) Post-annealing of the gel film in air at 800 °C for 4 h. The thicknesses of the film specimens are in the 250-300 nm range. The specimens contain grains with the size mostly in the 50-100 nm range observed by scanning electron microscopy.

The crystalline structure of the specimens was monitored by using XRD (Cu K_α line, wavelength = 0.15418 nm) in the grazing-incidence geometry with fixed X-ray incidence angle of 4°. The vibrational modes of the specimens were investigated by Raman spectroscopy employing a diode laser (wavelength = 514 nm, power = 1 mW). The XPS measurements on the specimens were performed using Al K_α line (photon energy = 1486.7 eV). The magnetic hysteresis curves of the specimens were measured at room temperature by using VSM in which the external magnetic field applied parallel to the film's plane was varied up to 15 kOe.

3. Results and Discussion

The crystalline properties of the $Mg_xCo_{1-x}Fe_2O_4$ specimens were investigated by XRD in comparison with $CoFe_2O_4$ as shown in Fig. 1. The XRD peak positions of the Mg-doped specimens are practically identical to those of the pristine $CoFe_2O_4$. The estimated lattice constants of the specimens based on the XRD data are close to 0.837 nm. The existence of Mg^{2+} ions in the specimens was probed by XPS of Mg 1*s* electrons, exhibiting a peak near the binding energy (BE) of 1303 eV, as shown in Fig. 2(a). In Fig. 2(b), the $2p_{3/2}$ and $2p_{1/2}$ peaks for Co ions are located at about 779.5 and 795.3 eV, respectively. The spin-orbit (s-o) energy splitting of 15.8 eV determined from the spectra implies that the Co ions in the specimens have valence of +2 [13]. In Fig. 2(c), the $2p_{3/2}$ and $2p_{1/2}$ peaks for Fe ions are peaked at about 710.5 and 723.9 eV,

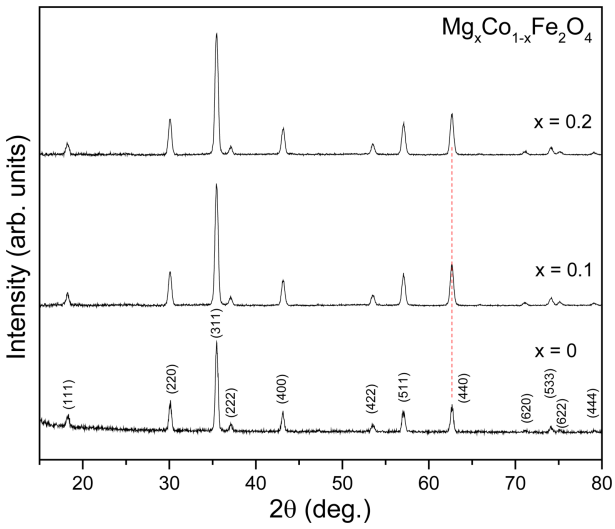

Fig. 1. X-ray diffraction patterns of thin-film $Mg_xCo_{1-x}Fe_2O_4$.

respectively. The 2*p* s-o splitting of 13.4 eV implies that the Fe ions in the specimens have valence of +3 [13]. All the peaks in the Fe 2*p* spectra (including satellites) are similar in shape and BE to those of α-Fe_2O_3 having Fe^{3+} ions [14, 15]. The satellites appeared in the 2*p* spectra of Fe^{3+} and Co^{2+} ions are attributable to the energy loss of the photoelectrons due to their interactions with high-spin 3*d* electrons in the ions [13]. The asymmetric shapes of the Fe and Co 2*p*-electron peaks in Figs. 2(b) and 2(c) imply that the peaks are composed of two origins, e.g., Fe^{3+}(B) and Fe^{3+}(A). The tetrahedral ions have higher BE than the octahedral ones by ~1 eV [16].

In Fig. 3, magnetic hysteresis loops of the $Mg_xCo_{1-x}Fe_2O_4$ specimens measured by using VSM are exhibited in comparison with those of $CoFe_2O_4$ and $Ca_xCo_{1-x}Fe_2O_4$ [12]. For the Mg-doped specimens, saturation magnetization (M_S) is larger than that of $CoFe_2O_4$ (415 emu/cm^3 = 79.3 emu/g), while coercivity (H_C) is smaller than that of $CoFe_2O_4$ (1.7 kOe). A similar magnetic behavior was reported for $Zn_xCoFe_{2-x}O_4$ powder specimens [2]. On the other hand, for $Ca_xCo_{1-x}Fe_2O_4$, M_S was smaller than that of $CoFe_2O_4$, while H_C was larger than that of $CoFe_2O_4$. The values of M_S, remanence (M_R), and H_C for the $Mg_xCo_{1-x}Fe_2O_4$ specimens are exhibited in comparison with those for $Ca_xCo_{1-x}Fe_2O_4$ in Figs. 4(a), 4(b), and 4(c), respectively. The values of M_S for $Mg_xCo_{1-x}Fe_2O_4$ are 561 and 510 emu/cm^3, respectively, for x = 0.1 and 0.2. For $Ca_xCo_{1-x}Fe_2O_4$, they were 379 and 303 emu/cm^3, respectively, for x = 0.1 and 0.2 [12]. The decrease (increase) in H_C for the Mg-doped (Ca-doped) specimens is attributable to the decrease (increase) in magnetic anisotropy. The magnetic anisotropy constant (K) can be estimated using the relation $M_SH_C = (0.96)K$, where M_S, H_C, and K have

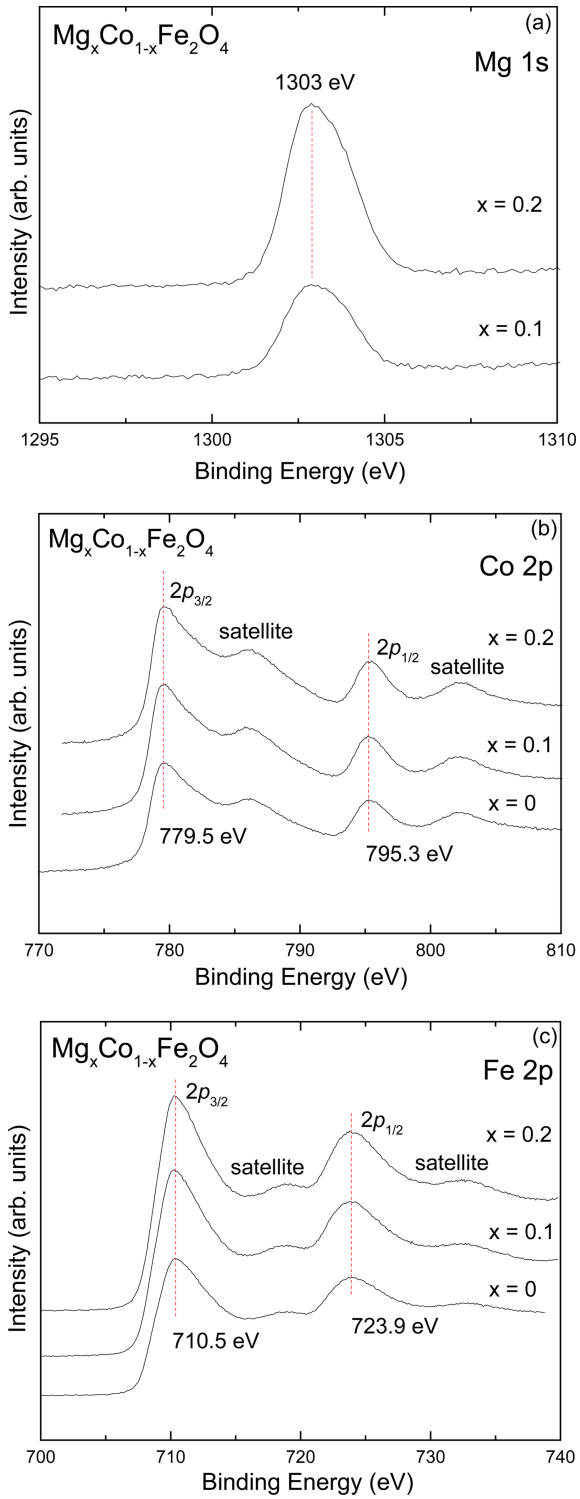

Fig. 2. (Color online) X-ray photoelectron spectra of (a) Mg 1*s*, (b) Co 2*p*, and (c) Fe 2*p* electrons of $Mg_xCo_{1-x}Fe_2O_4$ specimens.

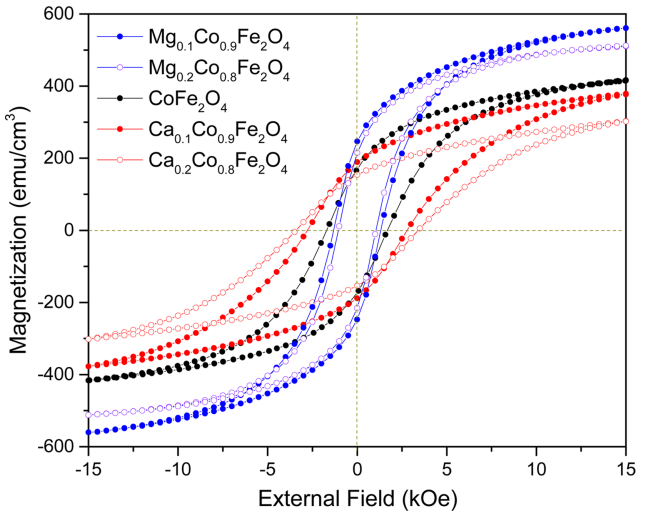

Fig. 3. (Color online) Magnetic hysteresis curves of $Mg_xCo_{1-x}Fe_2O_4$ specimens, exhibited in comparison with those of $Ca_xCo_{1-x}Fe_2O_4$ in Ref. 12.

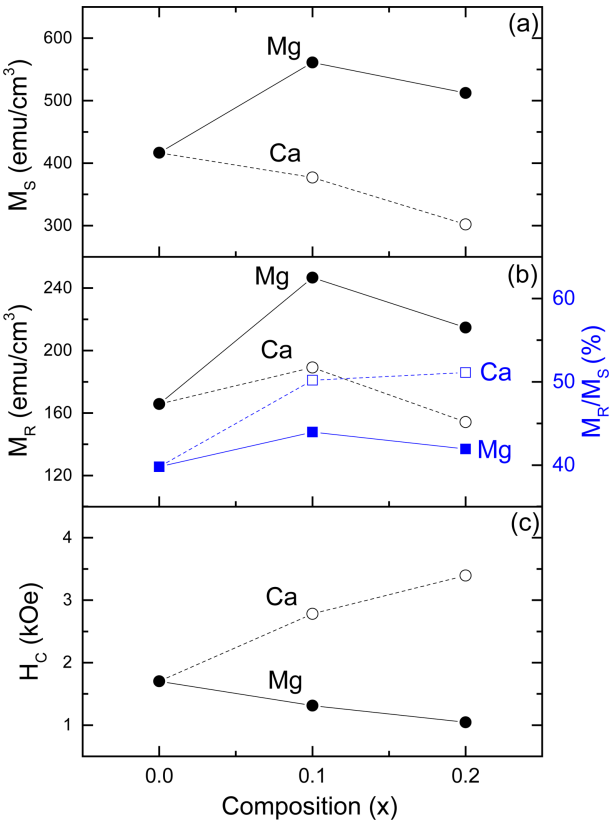

Fig. 4. (Color online) Magnetic parameters of $Mg_xCo_{1-x}Fe_2O_4$ specimens: (a) saturation magnetization (M_S), (b) remanence (M_R), and (c) coercivity (H_C), exhibited in comparison with those of $Ca_xCo_{1-x}Fe_2O_4$ in Ref. 12.

the unit of G [= $(4\pi)^{-1}$ emu/cm^3], Oe, and J/m^3, respectively [17]. The values of K for the $Mg_xCo_{1-x}Fe_2O_4$ specimens are 5.8×10^4 and 4.2×10^4 J/m^3, respectively, for x = 0.1 and 0.2. The anisotropy constants were 8.8×10^4 and 8.5×10^4 J/m^3 for x = 0.1 and 0.2, respec-

tively, for $Ca_xCo_{1-x}Fe_2O_4$ and 5.9×10^4 J/m^3 for $CoFe_2O_4$ [12]. The squareness ratio (M_R/M_S) is also shown in Fig. 4(b) along with the M_R data (circles). As the Mg and Ca composition increases, the hysteresis curves become more square-like with increasing demagnetization. The squareness ratio increases near to 0.5 with increasing x, implying that the domains are randomly oriented in the demagnetized state [17].

In Fig. 5, Raman spectra of the $Mg_xCo_{1-x}Fe_2O_4$ specimens are shown in thick black lines in comparison with $CoFe_2O_4$ and $Ca_xCo_{1-x}Fe_2O_4$ [12]. The distinction in the Raman spectra between $Mg_xCo_{1-x}Fe_2O_4$ and $Ca_xCo_{1-x}Fe_2O_4$ is the intensity (I_A) of a peak located near 615 cm^{-1} as indicated by arrows. For $Mg_xCo_{1-x}Fe_2O_4$, I_A is larger than that of the neighboring peak near 580 cm^{-1} as indicated by *, while the former is smaller than the latter for $Ca_xCo_{1-x}Fe_2O_4$. The 615-cm^{-1} peak is ascribed to A_{1g} phonon mode for symmetric stretching vibration of O^{2-} ions surrounding tetrahedral Co^{2+} ion, denoted by $A_{1g}(Co^{2+})$ [18, 19]. So, the change in I_A is likely to indicate the change in tetrahedral Co^{2+} density. The peak located near 693 cm^{-1} is ascribed to A_{1g} mode related to tetrahedral Fe^{3+} ion, denoted by $A_{1g}(Fe^{3+})$ [18]. The peaks at the lower energies are ascribed to T_{2g} (580, 470, 207 cm^{-1}) and E_g (305 cm^{-1}) phonon modes for symmetric and anti-symmetric bending vibrations, respectively, of O^{2-} ions surrounding the octahedral cations [18]. The sharp peak at 520 cm^{-1} is ascribed to the Si substrate of the film.

Among the three T_{2g} peaks, the one near 470 cm^{-1} (indicated by **) is the strongest. Such a peak is known to be absent in Raman spectra of Fe_3O_4 [20, 21], for which single A_{1g} peak was observed near 670 cm^{-1}. Thus, the 470-cm^{-1} T_{2g} mode is ascribed to octahedral Co^{2+} ions [18], denoted by $T_{2g}(Co^{2+})$. The change in the intensity (I_B) of the 470-cm^{-1} peak is likely to indicate the change in octahedral Co^{2+} density. Thus, the Raman spectra of $Co_{1-x}T_xFe_2O_4$ (T = Mg and Ca) turn out to show phonon modes involving both tetrahedral (615 cm^{-1}) and octahedral (470 cm^{-1}) Co^{2+} ions [18]. The intensity ratio (I_A:I_B) between 615-cm^{-1} and 470-cm^{-1} peak can be an indicative of the relative population of Co^{2+} ions between the A and B site.

The relative Co^{2+} population at the A and B sites of the specimens was estimated by curve-fitting the Raman spectra, as shown in Fig. 5, where the fitted curves of the spectra are shown as thin colored lines below the experimental data (thick black line). The areal ratio between the 615 cm^{-1} (I_A) and 470 cm^{-1} (I_B) peaks is likely to represent the relative population of Co^{2+} ions between the A and B site. For the $Mg_xCo_{1-x}Fe_2O_4$ specimens, the intensity ratio (I_A:I_B) turned out to be 38:62 and 36:64 for

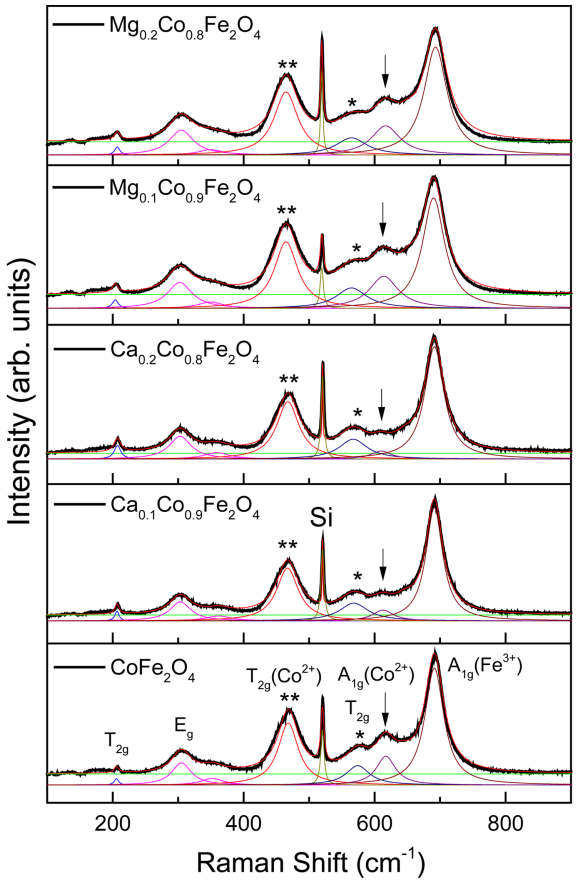

Fig. 5. (Color online) Raman spectra of $Mg_xCo_{1-x}Fe_2O_4$ specimens, exhibited in comparison with those of $Ca_xCo_{1-x}Fe_2O_4$ in Ref. 12. Experimental data are drawn in black and thick-solid lines. Colored and thin-solid lines below the experimental curve represent the result of curve-fitting on the experimental data.

x = 0.1 and 0.2, respectively. Compared to $CoFe_2O_4$ (30:70), the A site occupancy of Co^{2+} ion is found to increase through the Mg doping. The Mg^{2+} substitution in the spinel lattice appears to boost Co^{2+} occupation in the A site. On the other hand, for $Ca_xCo_{1-x}Fe_2O_4$, the intensity ratio was 16:84 and 11:89 for x = 0.1 and 0.2, respectively [12], implying a reduction of the A site occupancy of Co^{2+} ion compared to $CoFe_2O_4$. Thus, the Raman spectral analyses predict the opposite behavior of Co^{2+} ions between the Mg^{2+} and Ca^{2+} substitution in $CoFe_2O_4$ although the two elements belong to the same group (II) in the periodic table.

The ionic distribution among the A and B sites for the Mg-substituted compounds can be described as $(Co^{2+}{}_{1-\delta}\ Mg^{2+}{}_{x-y}\ Fe^{3+}{}_{\delta})^A[Co^{2+}{}_{\delta-x}\ Mg^{2+}{}_{y}\ Fe^{3+}{}_{2-\delta}]^BO_4$ for x = 0.1 and 0.2. There have been reports in which Mg^{2+} ions can occupy both the A and B sites of the spinel ferrites [11, 22]. For $Ca_xCo_{1-x}Fe_2O_4$, the decrease of M_S with increasing

x could be explained by assuming B-site dominance of the Ca^{2+} ions. However, the increase of M_S for $Mg_xCo_{1-x}Fe_2O_4$ compared to $CoFe_2O_4$ suggests that Mg^{2+} ions occupy both the A- and B-sites. The A-site occupation of non-magnetic Mg^{2+} ions may induce the migration of high-spin Fe^{3+} ions from A- to B-sites, leading to an increase of the net magnetic moment of the ferrimagnetic formula unit.

For x = 0.2 of $Mg_xCo_{1-x}Fe_2O_4$, the Raman intensity ratio (I_A:I_B) is estimated to be 36:64, which leads to the Co^{2+} compositions of 0.29 and 0.51 for the A- and B-sites, respectively. Assuming that 75 % and 25 % of the Mg^{2+} ions occupy the A- and B-sites, respectively, the ionic distribution for x = 0.2 becomes $(Co^{2+}_{0.29}\,Mg^{2+}_{0.15}\,Fe^{3+}_{0.56})^A[Co^{2+}_{0.51}\,Mg^{2+}_{0.05}\,Fe^{3+}_{1.44}]^BO_4$, leading to δ = 0.56. The inversion parameter for x = 0.2 is smaller than that of $CoFe_2O_4$ (δ = 0.7) [5, 6]. For $Ca_xCo_{1-x}Fe_2O_4$, it was estimated to be 0.91 for x = 0.2 where the Co^{2+} compositions are 0.09 and 0.71 for the A- and B-sites, respectively [12]. The magnetic moment per formula unit of $Mg_xCo_{1-x}Fe_2O_4$ (x = 0.2) is estimated to be 5.1 μ_B. It is larger by 20 % than that of $CoFe_2O_4$ (4.2 μ_B). In the calculation, the magnetic moments of Co^{2+} and Fe^{3+} ions are assumed to be 3 and 5 μ_B, respectively, while the Mg^{2+} ion is assumed to contribute no magnetic moment. Thus, the theoretical estimation under the assumption of 3:1 for A:B occupation ratio of Mg^{2+} ions is in good agreement with the experimental result: M_S of $Mg_{0.2}Co_{0.8}Fe_2O_4$ (510 emu/cm^3) is larger than that of $CoFe_2O_4$ (415 emu/cm^3) by 20 %. The calculation under the assumption that all the Mg^{2+} ions occupy the B sites, $(Co^{2+}_{0.29}\,Fe^{3+}_{0.71})^A[Co^{2+}_{0.51}\,Mg^{2+}_{0.2}\,Fe^{3+}_{1.29}]^BO_4$, produces the magnetic moment of 4.1 μ_B. It is smaller than that of $CoFe_2O_4$, so does not agree with the experimental result. Thus, the large M_S values of $Mg_xCo_{1-x}Fe_2O_4$ can be understood in terms of the tetrahedral preference of Mg^{2+} ions in the spinel lattice.

4. Conclusions

The magnetic hysteresis properties of $Mg_xCo_{1-x}Fe_2O_4$ ($x \leq 0.2$) ferrites are significantly different from those of $Ca_xCo_{1-x}Fe_2O_4$, although Mg and Ca belong to the same group (II) in the periodic table. The values of M_S for $Mg_xCo_{1-x}Fe_2O_4$ ferrites are larger than that of $CoFe_2O_4$, while the values of H_C are smaller than that of $CoFe_2O_4$. For $Ca_xCo_{1-x}Fe_2O_4$ ferrites, on the other hand, M_S and H_C vary oppositely to those of $Mg_xCo_{1-x}Fe_2O_4$. The Raman spectral analyses indicate that the Mg-substituted (Ca-substituted) ferrites have higher (lower) tetrahedral Co^{2+} density than $CoFe_2O_4$. The increase of M_S for $Mg_xCo_{1-x}Fe_2O_4$ compared to $CoFe_2O_4$ is ascribed to (i) the increase of tetrahedral Co^{2+} density and (ii) the tetrahedral preference of Mg^{2+} ions.

Acknowledgment

This work was supported by Incheon National University Research Grant in 2020.

References

[1] M. M. Yallapu, S. F. Othman, E. T. Curtis, B. K. Gupta, M. Jaggi, and S. C. Chauhan, Biomaterials **32**, 1890 (2011).
[2] N. Somaiah, T. V. Jayaraman, P. A. Joy, and D. Das, J. Magn. Magn. Mater. **324**, 2286 (2012).
[3] D. Mandal and K. Mandal, J. Magn. Magn. Mater. **536**, 168127 (2021).
[4] J. S. Sagu, K. G. U. Wijayantha, and A. A. Tahir, Electrochim. Acta **246**, 870 (2017).
[5] D. Carta, M. F. Casula, A. Falqui, D. Loche, G. Mountjoy, C. Sangregorio, and A. Corrias, J. Phys. Chem. C **113**, 8606 (2009).
[6] K. J. Kim and J. Park, J. Sol-Gel Sci. Technol. **92**, 40 (2019).
[7] S. Nappini, E. Magnano, F. Bondino, I. Pis, A. Barla, E. Fantechi, F. Pineider, C. Sangregorio, L. Vaccari, L. Venturelli, and P. Baglioni, J. Phys. Chem. C **119**, 25529 (2015).
[8] J. Venturini, A. M. Tonelli, T. B. Wermuth, R. Y. S. Zampiva, S. Arcaro, A. D. C. Viegas, and C. P. Bergmann, J. Magn. Magn. Mater. **482**, 1 (2019).
[9] A. L. Gurgel, A. E. Martinelli, O. L. A. Conceicao, M. M. Xavier, M. A. M. Torres, and D. M. A. Melo, J. Alloys Comp. **799**, 36 (2019).
[10] B. G. Souza, G. Figueira, M. H. Carvalho, V. Alcaraz-Gonzalez, K. E. Saldana-Flores, M. Godinho, A. J. A. Oliveira, R. H. G. A. Kiminami, L. A. M. Ruotolo, and E. A. Urquieta-Gonzalez, Mater. Chem. Phys. **257**, 123741 (2021).
[11] S. V. Bhandare, R. Kumar, A. V. Anupama, M. Mishra, R. V. Kumar, V. M. Jali, and B. Sahoo, Mater. Chem. Phys. **251**, 123081 (2020).
[12] K. J. Kim, J. Park, and J. Y. Park, J. Magn. **26**, 410 (2021).
[13] W. Bian, Z. Yang, P. Strasser, and R. Yang, J. Power Sources **250**, 196 (2014).
[14] T. Droubay and S. A. Chambers, Phys. Rev. B **64**, 205414 (2001).
[15] K. J. Kim, J. Park, and J. Y. Park, J. Magn. **27**, 96 (2022).
[16] T. Fujii, F. M. F. de Groot, G. A. Sawatzky, F. C. Voogt, T. Hibma, and K. Okada, Phys. Rev. B **59**, 3195 (1999).
[17] H. Yang, Z. Wang, L. Song, M. Zhao, J. Wang, and H. Luo, J. Phys. D: Appl. Phys. **29**, 2574 (1996).

[18] V. Georgiadou, V. Tangoulis, I. Arvanitidis, O. Kalogirou, and C. Dendrinou-Samara, J. Phys. Chem. C **119**, 8336 (2015).
[19] R. S. Yadav, I. Kuritka, J. Vilcakova, J. Havlica, J. Masilko, L. Kalina, J. Tkacz, J. Svec, V. Enev, and M. Hajduchova, Adv. Nat. Sci.: Nanosci. Nanotechnol. **8**, 045002 (2017).
[20] I. Chamritski and G. Burns, J. Phys. Chem. B **109**, 4965 (2005).
[21] K. J. Kim, T. Y. Koh, J. Park, and J. Y. Park, J. Magn. **22**, 360 (2017).
[22] H. R. Dakua, N. Venkataramani, and S. Prasad, AIP Adv. **6**, 055919 (2016).